AGU PUBLICATIONS

JGR

Journal of Geophysical Research: Atmospheres

RESEARCH ARTICLE
10.1002/2014JD022062

Key Points:
- Potential dust sources are computed online in a global climate-aerosol model
- For today's climate 10% of dust particles are emitted from agricultural areas
- Changes in climate and land use contributed equally to changes in dust burden

Supporting Information:
- Readme
- Figures S1–S8

Correspondence to:
T. Stanelle,
tanja.stanelle@env.ethz.ch

Citation:
Stanelle, T., I. Bey, T. Raddatz, C. Reick, and I. Tegen (2014), Anthropogenically induced changes in twentieth century mineral dust burden and the associated impact on radiative forcing, *J. Geophys. Res. Atmos.*, *119*, 13,526–13,546, doi:10.1002/2014JD022062.

Received 23 MAY 2014
Accepted 20 NOV 2014
Accepted article online 25 NOV 2014
Published online 12 DEC 2014

Anthropogenically induced changes in twentieth century mineral dust burden and the associated impact on radiative forcing

Tanja Stanelle[1], Isabelle Bey[1], Thomas Raddatz[2], Christian Reick[2], and Ina Tegen[3]

[1]Center for Climate System Modeling, ETH Zurich, Zurich, Switzerland, [2]Max Planck Institute for Meteorology, Hamburg, Germany, [3]Leibniz Institute for Tropospheric Research, Leipzig, Germany

Abstract We investigate the relative importance of climate change (CC) and anthropogenic land cover change (ALCC) for the dust emissions and burden changes between the late nineteenth century and today. For this purpose, the climate-aerosol model ECHAM6-HAM2 is complemented by a new scheme to derive potential dust sources at runtime using the vegetation cover provided by the land component JSBACH of ECHAM6. Dust emissions are computed online using information from the ECHAM6 atmospheric component. This allows us to account for changes in land cover and climate interactively and to distinguish between emissions from natural and agricultural dust sources. For today's climate we find that nearly 10% of dust particles are emitted from agricultural areas. According to our simulations, global annual dust emissions have increased by 25% between the late nineteenth century and today (e.g., from 729 Tg/a to 912 Tg/a). Globally, CC and ALCC (e.g., agricultural expansion) have both contributed to this change (56% and 40%, respectively). There are however large regional differences. For example, change in dust emissions in Africa are clearly dominated by CC. Global dust burden have increased by 24.5% since the late nineteenth century, which results in a clear-sky radiative forcing at top of the atmosphere of $-0.14\ W/m^2$. Based on these findings, we recommend that both climate changes and anthropogenic land cover changes should be considered when investigating long-term changes in dust emissions.

1. Introduction

Mineral dust particles are a key component of the atmospheric aerosol phase, as they can impact the Earth's radiative budget, precipitation processes, atmospheric chemistry, and biogeochemistry [e.g., *Forster et al.*, 2007; *Dentener et al.*, 1996; *Jickells et al.*, 2005]. In addition, they affect local air quality and pose a potential health risk [*Clausnitzer and Singer*, 1996]. Aerosols dominate the uncertainty in total anthropogenic radiative forcing. Particularly uncertain is the contribution from dust originating from agricultural activities [*Tegen et al.*, 2002; *Ginoux et al.*, 2012; *Boucher*, 2013] that we investigate in the present study.

Mineral dust particles are usually considered as "natural" aerosols as they are mainly produced by wind-induced processes (saltation, etc.) over arid or semiarid regions characterized by sparse vegetation. While it is recognized that the main large dust source regions correspond to dried paleolakes [*Prospero et al.*, 2002; *Ginoux et al.*, 2001; *Tegen et al.*, 2002], there are still large uncertainties about the global and regional source regions and strength [*Huneeus et al.*, 2011]. In particular, the extent to which human activities affect emission of dust particles by altering land properties and use (e.g., increase in agricultural surfaces) or indirectly by climate change (e.g., change in wind and precipitations patterns) remains poorly quantified [*Zender et al.*, 2004; *Boucher*, 2013]. Modeling studies suggest that human activities have contrasting impacts on dust burden changes since preindustrial times, e.g., human land use, carbon dioxide fertilization, and climate change can either increase or decrease dust emissions [*Mahowald and Luo*, 2003]. Estimates of the net effect of human activities on today's dust emissions range between −20% to +60% [*Tegen and Fung*, 1995; *Prospero et al.*, 2002; *Mahowald and Luo*, 2003; *Tegen et al.*, 2004; *Mahowald et al.*, 2004; *Moullin and Chiapello*, 2006; *Mahowald et al.*, 2009, 2010; *Ginoux et al.*, 2012].

The contribution of agricultural areas to the global dust budget remains quite uncertain. *Tegen et al.* [2004] used dust storm observations to conclude that dust from agricultural areas contributes less than 10% to the global dust load. Using the same observational data set, *Mahowald et al.* [2004] found that anthropogenic contribution to global dust emissions ranges from 0 to 50%. *Ginoux et al.* [2012] estimated that natural dust

sources represent 75% of global emissions based on the Moderate Resolution Imaging Spectrometer (MODIS) Deep Blue level 2 data. They further estimated that 20% of emissions originated from vegetated surfaces, primary desert shrublands, and agricultural lands. As a result of these uncertainties, the range of the radiative forcing attributed to anthropogenic dust particles remains large ($-0.1 \pm 0.2\,W/m^2$) [*Forster et al*., 2007; *Boucher*, 2013].

In this context, the goal of our study is to quantify the impact of human activities on changes in dust emissions and burden between 1880 and today. In contrast to previous studies [e.g., *Neff et al*., 2008; *Mahowald et al*., 2010; *Mulitza et al*., 2010], we aim to distinguish between the effect of climate change (CC) and anthropogenic land cover change (ALCC). We focus on two time periods, namely the decades of the 1880s and 2000s, because (i) the human influence on both climate (e.g., change in global temperature) and land cover (e.g., the areas used for agricultural purposes) increased significantly especially after 1880 [e.g., *Hurtt et al*., 2011] and (ii) a suite of in situ and satellite observations are now available for the last decade well suitable for model evaluation.

We use the global aerosol-climate model ECHAM6-HAM2.1 (version: ECHAM6.1.0-HAM2.1-MOZ0.8), augmented with a new method to calculate potential dust source areas that directly links the dust emission scheme to the land component of the climate model (section 2). Results of the modified model version are evaluated against satellite and ground-based measurements for today's climate and compared with other model results (section 3). We conduct a series of sensitivity simulations to disentangle the role of climate change (CC) and anthropogenic land cover change (ALCC) for dust formation, and the associated radiative forcing since the late nineteenth century (section 4). Summary and conclusion are provided in section 5. This study is a first step toward a comprehensive understanding of the land-atmosphere interactions occurring through aerosols.

2. Model Description

Our study employs ECHAM6-HAM2.1. This is the latest version of the ECHAM-HAM model family, which was first described by *Stier et al*. [2005]. It is based on the newest versions of both the ECHAM6 global circulation model [*Stevens et al*., 2013] and the aerosols module HAM2 [*Zhang et al*., 2012]. A short description is provided in the following but the focus is put on the description of the dust emission module that was modified for this study.

Aerosol microphysics is simulated using the M7 module [*Vignati et al*., 2004], which accounts for sulfate, black carbon, particulate organic matter, sea salt, and dust. The atmospheric aerosol population is described as a superposition of seven lognormal distributed modes for which standard deviations are prescribed. The total number concentration and masses of the different chemical components are prognostic variables in the model. The modes are divided into soluble, internally mixed modes (containing sulfate) and insoluble, externally mixed modes, which are assigned to different size ranges. The modal diameters can vary and are calculated at each time step from the mass and number concentrations for each mode. Dust particles are considered as part of the soluble and insoluble accumulation and coarse modes. Sedimentation and dry and wet deposition are parameterized as functions of the aerosol size distribution, composition, and mixing state and depend on the ECHAM6 meteorology. The emission fluxes of dust, sea salt, and dimethyl sulfide from the oceans are calculated online, based on the model meteorology. Anthropogenic emissions are prescribed.

Aerosols interact with the climate model through the direct, indirect, and semidirect aerosol effect. Using a look-up table precalculated according to Mie theory, the radiative properties of aerosols are dynamically computed based on their chemical composition, water content, and size of the particles [*Stier et al*., 2005; *Zhang et al*., 2012]. The simulated aerosol population is linked to the number concentrations of cloud droplet and ice crystal through the aerosol activation and ice nucleation parameterization of the two-moment cloud scheme [*Lohmann et al*., 2007].

2.1. Dust Emission Scheme

2.1.1. Dust Source Scheme

In the standard version of ECHAM6-HAM2.1, the dust source scheme of *Tegen et al*. [2002] including improvements of *Cheng et al*. [2008] is used. The dust scheme is coupled online with the atmospheric component of the climate model [*Stier et al*., 2005]. Emission of dust particles is driven by the 10 m wind

speed, following a nonlinear physical process, which depends on surface features and meteorological conditions in potential source areas.

The total emission flux is calculated from 192 dust size classes, which range from 0.2 to 1300 μm in diameter and are grouped into three lognormal size distributions. For each of the size classes, an individual threshold friction velocity is calculated after *Marticorena et al*. [1997]. We assume a constant low roughness length of 0.001 cm in areas where dust emissions are possible. Each grid box includes specific portions of four different soil types: clay, silt, medium/fine sand, and coarse sand. The explicit formulation of the saltation process follows *Marticorena and Bergametti* [1995]. A ratio between vertical and horizontal emission fluxes is prescribed for each soil type [*Tegen et al*., 2002]. The vertical emission fluxes are further integrated over the 192 internal size classes. The fluxes are attributed to two aerosol modes, including the insoluble accumulation mode (mass mean radius (mmr) = 0.37 μm, standard deviation (sigma) = 1.59) and the coarse mode (mmr = 1.75 μm, sigma = 2) for the subsequent simulation of aerosol microphysics, advection, and deposition processes in the model. Emission into the supercoarse mode is neglected because of their short lifetime [*Stier et al*., 2005; *Cheng et al*., 2008].

2.1.2. Determination of Potential Dust Source Areas in the ECHAM6-HAM2.1 Standard Version

Places where emissions of dust particles could take place if certain criteria are fulfilled (e.g., friction velocity larger than threshold) are called potential dust source areas. In general, nonvegetated or low-vegetated areas are potential dust source areas. In the standard ECHAM6-HAM model the distribution of potential dust source regions is taken from an external file derived by *Tegen et al*. [2002], who identified potential dust source areas using the satellite-derived fraction of absorbed photosynthetic active radiation (FAPAR) and a model-derived distribution of potential vegetation types. FAPAR is derived from monthly retrievals of the normalized difference vegetation index measured by the Advanced Very High Resolution Radiometer satellite instrument [*Braswell et al*., 1997] for "current" climate (1982–1993).

While this methodology provides a reasonable estimate of current dust sources, it has several shortcomings. For example, interannual variability in vegetation cover is not considered and only natural dust sources are taken into account. In addition, the vegetation model, which is used to calculate the distribution of potential vegetation types, is not the same as in ECHAM6, which prevents the investigation of interactions and couplings in the climate system over long periods in a comprehensive manner. In the following, we present a new approach to determine potential dust sources, whose goal is to provide a direct link between the dynamically developing land cover in the land component of ECHAM6 and the dust emission scheme.

2.1.3. Modifications to the Dust Emission Scheme Introduced in This Work

We take advantage of the online coupling between the land component JSBACH and the atmospheric component in the ECHAM6 model. In JSBACH a grid box is first divided into two parts, one representing bare soil and the other being covered with vegetation. This vegetated fraction of the grid box is further subdivided into tiles, one for each of the 11 PFTs (Plant Functional Types) distinguished in JSBACH. Each PFT covers a fraction $f_{\mathrm{veg}}(\mathrm{PFT})$ of the vegetated part of the grid box. Our new approach relies on the following assumptions:

1. The fraction of a grid box not covered with vegetation ($f_{\mathrm{bare\ soil}}$) is a potential dust source.
2. Dust cannot be emitted from areas covered with trees.
3. Gaps in low-stature vegetation (natural grasslands, shrubs, tundra, swamps, crops, and pastures) are assumed to be potential sources for dust emissions. In contrast, gaps in forests are too well protected for dust activation. As usually done in JSBACH, the gap fraction of the area covered by a particular PFT in a grid cell is computed as

$$f_{\mathrm{gap}}(\mathrm{PFT}) = \exp\left(-\mathrm{LAI}_{\mathrm{max}}(\mathrm{PFT})/b_{\mathrm{clump}}(\mathrm{PFT})\right)$$

where $\mathrm{LAI}_{\mathrm{max}}$ is the maximum value of the leaf area index of the particular PFT and b_{clump} is a clumpiness factor ($b_{\mathrm{clump}} = 2$ for all PFTs except for crops $b_{\mathrm{clump}} = 3$). Both are standard parameters of JSBACH.

4. For crops we assume in addition that dust emissions are prevented only during the growing season, i.e., between sowing and harvest, which we define as times with $\mathrm{LAI} > 0.2$. Formally, we introduce this mechanism by setting $f_{\mathrm{gap}}(\mathrm{crops}) = 1$ when $\mathrm{LAI} \leq 0.2$.
5. Snow cover prevents dust emissions. The fraction of a grid cell covered with snow is denoted here by f_{snow}.

6. A special assumption is necessary to handle lakes because in ECHAM an inland grid cell is either land or lake, according to whether the fraction of open water bodies (f_{lake}) is less or larger 50% of grid cell area. To compensate for this simplification in continental area, we choose to correct for a possible overestimation of dust emissions in the land cells, but to ignore a possible underestimation in the lake cells. Accordingly, we decrease the dust emitting area of a land grid cell by the factor $1 - f_{lake}$.

   Summarizing all assumptions so far, the fraction f_{pot} (PFT) of grid cell covered by a specific PFT being a potential dust source is thus calculated as

$$f_{pot}(\mathrm{PFT}) = (1 - f_{snow}) \cdot (1 - f_{lake}) \cdot (1 - f_{bare\ soil}) \cdot f_{gap}(\mathrm{PFT}) \cdot f_{veg}(\mathrm{PFT})$$

   The fraction of a grid cell covered by bare soil acting as a potential dust source ($f_{pot,\ bare\ soil}$) is given by

$$f_{pot,\ bare\ soil} = (1 - f_{snow})(1 - f_{lake}) \cdot f_{bare\ soil}$$

   Finally, two additional considerations need to be described:

7. Dust is not entrained when the upper most centimeters of the soil are wet. Our JSBACH version uses a bucket model for simulating soil moisture, i.e., no information is available about the vertical profile of soil moisture. For this reason we use the skin water reservoir as a measure of surface soil wetness. It has a maximum value around 10^{-3} cm. Since even a weak rain event is filling it completely, we do not interpolate the ability for dust emissions between a full and empty skin reservoir. For numerical reasons we assume the reservoir to be empty when its filling is less than 10^{-6} cm; in that case dust emission becomes possible.
8. A final but—for our study—important assumption concerns the extent to which agricultural lands act as potential dust source areas. Based on their findings *Neff et al.* [2005] suggested that cultivation and grazing make soils much more vulnerable to erosion, indicating that dust emission can easily take place in agricultural areas. However, farmers partly employ several types of soil conservation techniques (like planting of windbreaks, contour plowing, and leaving plant residuals as soil cover at the fields) that effectively reduce wind erosion and thus decrease dust emission in agricultural areas [*Baker et al.*, 2005], especially the history of dust storms from the Great Plains in the U.S. as compared to Texas tells about the efficiency of soil conservation [*Lee et al.*, 1993]. During the 1930s the Great Plains experienced severe droughts. As a consequence huge dust storms developed over part of the Great Plains that were later on dubbed "Dust Bowl." Large parts of the Dust Bowl area are farmlands but soil conservation techniques were only rarely applied. In contrast, farmers in Texas systematically took care of soil conservation and the even more severe and long drought during the 1950s did not result in such severe dust storms as in the Great Plains. Today, windbreaks are an important element of the Great Plains landscape [*Nordstrom and Hotta*, 2004]. Velocity reductions for average tree windbreaks can reach up to 60%–80% close to the barrier and about 20% downwind of the barrier [*Tibke*, 1988]. Another method for preventing soil erosion is tilling. Subsoil in dry regions can remain moist for long periods and have higher clay content than the surface soil. Bringing subsoil to the surface can reduce erosion [*Bunn*, 1997]. *Grantz et al.* [1998] found that the threshold wind friction velocity for dust emission increases from 45 cm/s to 65 cm/s (approximately 40%) due to tillage. *Uri* [1999] estimated that conservation tillage was used on nearly 36% of planted land in the U.S. in 1996. Based on in situ measurements, *Gillette* [1988] showed that the increase in the threshold friction velocity due to agricultural practices also depends on the soil texture. He found that the increase is less pronounced for sandy soils and maximal for loamy soils. But for simplicity we decided to account for tilling by generally increasing the threshold friction velocity by 40% for all croplands rather than accounting for soil type.

Finally, the dust fluxes in each vegetated part of the grid box D_{pft},(PFT), and in the bare soil part of the grid box D_{bare} are calculated following *Tegen et al.* [2002] (see also section 2.1.1). The total dust flux D_{tot} in each grid box is then given by

$$D_{tot} = D_{bare} \cdot f_{pot,bare\ soil} + \sum_{PFT} D_{PFT}(\mathrm{PFT}) \cdot f_{pot}(\mathrm{PFT})$$

These emission fluxes are then used in the standard HAM model to simulate the behavior of these dust aerosols in the atmosphere.

2.2. Simulation Setup

We employed our model in two different setups. For the evaluation of our modified model system (section 3), we performed nudged simulations for the period 2005–2009 at T63L31 resolution (approximately 200 km × 200 km)

Table 1. Characterization of Unnudged Simulations[a]

Name	Climate of Years	Land Cover of Years
pCpL	2000–2010	2000–2010
hChL	1880–1890	1880–1890
pChL	2000–2010	1880–1890
hCpL	1880–1890	2000–2010

[a]pC stands for present climate, hC for historical climate, pL for present land use, and hL for historical land use.

using the ERA-Interim meteorological reanalysis data. Emissions of anthropogenic aerosols are taken from the MACCity emission inventory [*Granier et al*., 2011], which is derived from the Atmospheric Chemistry and Climate Model Intercomparison Project data set [*Lamarque et al*., 2010]. The distribution of natural vegetation land cover is prescribed from maps derived by *Ramankutty and Foley* [1999] and modified by anthropogenic land cover change data from *Hurtt et al*. [2011] as implemented by *Reick et al*. [2013]. We prescribe sea surface temperature (SST) and sea ice concentration (SIC) from the Atmospheric Model Intercomparison Project 2 data set [*Fiorino*, 2000]. Greenhouse gas concentrations are taken from *van Vuuren et al*. [2011]. We performed two different simulations, namely, a simulation with the standard version of ECHAM6-HAM2.1 (referred to as STD) and a simulation including our new approach with the modified potential dust source areas (referred to as NEW). A global correction factor (0.83) on the threshold friction velocity for dust emission is applied in both simulations. Such a nonphysical correction factor is used in global models to account for the inhomogeneity of the factors influencing dust emissions (e.g., surface wind) across the rather coarse-model grid boxes in such simulations [e.g., *Zender et al*., 2003; *Ridley et al*., 2013].

In section 4 we analyze the separate importance of CC and ALCC for changes in dust burden between the late 19th century and the beginning of the 21st century. For this purpose, we performed 10 year free running (which means that the simulation is not nudged to a prescribed state) simulations in T63L31 resolution. The model setup is identical to the NEW simulation described above unless indicated in the following. In all free simulations, we use a global correction factor of 0.95 for lowering the threshold friction velocity for dust emissions. This global correction factor is slightly higher than in the nudged simulations to account for the fact that wind speeds are in general higher in free running simulations [*Timmreck and Schulz*, 2004].

In section 4 we compare simulation results for the decade 2000–2010 (referred to as present (p)) with results for the decade 1880–1890 (referred to as historic (h) in the following). To disentangle the effects from CC and ALCC, we performed sensitivity simulations with our modified ECHAM6-HAM2.1 model system using all possible combinations of land cover and climate for the historic and present decades (see Table 1). By comparing the two simulations "pCpL" (present climate + present land cover) and "hChL" (historical climate + historical land cover), one obtains the changes in dust emissions, burdens, and the associated impact on radiative forcing from the combined effect of CC and ALCC between the late nineteenth century and today. By comparing additional sensitivity simulations (pChL: present climate + historical land cover; and hCpL: historical climate + present land use) to the pCpL simulation, one is able to distinguish between the relative influence of ALCC and CC.

Further, we performed four additional nudged 1 year simulations for present-day conditions in which we prescribed dust emission flux using 10 year mean monthly emission fluxes archived from the four free running simulations described previously. Radiative forcing is then calculated using a double call to the radiation scheme, with the second call not accounting for aerosol optical properties. In the remainder of the manuscript, we refer to radiative forcing as being the difference between the two calls. Since the two simulations differ only by the prescribed dust emissions, this is the radiative forcing due to change in dust burden.

3. Evaluation of the Modified Dust Emission Model for Today's Climate

In this section, we perform a detailed evaluation of the new dust emission model using a suite of satellite and in situ observations. Recall that our new approach aims at deriving a method for the calculation of the global distribution of potential dust source areas, which (i) is more independent of external information (e.g., satellite data of land cover) and (ii) allows to distinguish between natural and anthropogenic dust sources. This will, in turn, allow us to investigate the consequences of changing land cover on dust emissions for past and future climate when land cover observations are not available (see section 4). This implies that, for

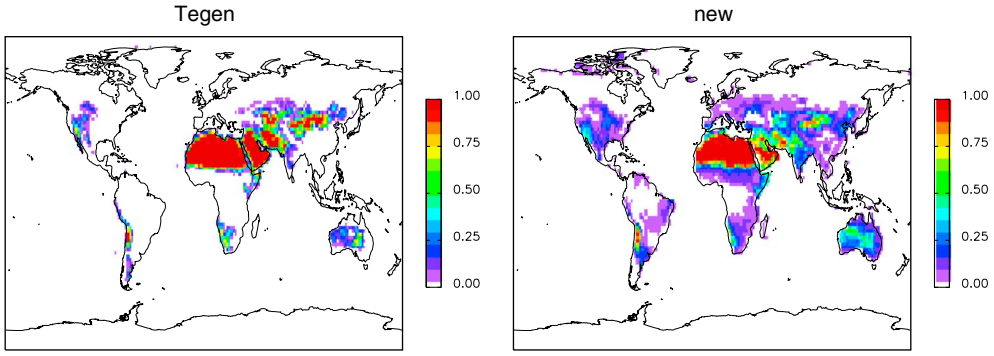

Figure 1. Fraction of grid box, which acts as potential dust source as derived in (left) *Tegen et al*. [2002] and (right) our method.

today's climate, we do not necessarily expect that our new approach results in a substantial improvement over the standard dust scheme of *Tegen et al*. [2002], which relies on potential dust source areas derived from satellite data.

3.1. Potential Dust Source Areas

Figure 1 compares the yearly mean distribution of potential dust sources from the STD and NEW simulations. The extent of potential dust sources is larger in simulation NEW, especially in regions dominated by agricultural land use like Europe, the Sahel, and the Great Plains in the U.S., although emissions are typically low in these regions. In contrast, the high-emission regions are largely identical in both simulations. This is true in particular for the so-called "Dust Belt" [*Prospero et al*., 2002] extending from the Sahara through the Middle East and Central Asia to China, which is present in both simulations. Other regions such as the Great Plains in the U.S. and much of Australia which were previously identified as potential dust source areas, for example, by *Koven and Fung* [2008] and *Ginoux et al*. [2012], are also found in the NEW simulation.

Shannon and Lunt [2011] determined dust source areas from simulations with the Lund Potsdam Jena vegetation model. They found, similarly to us, large dust source areas in the Canadian Arctic. To distinguish between polar and hot deserts, they introduced a threshold in their parameterization for annual growing days (number of days when daily temperature is greater than 5°C) whereby they limit dust emissions at high latitudes so that polar deserts do not act as dust source by their parameterization. However, we prefer not to apply any artificial criteria to limit high-latitude dust emissions.

3.2. Global Mineral Dust Budget

In the context of the AeroCom initiative, *Huneeus et al*. [2011] intercompared different dust simulations (including an ECHAM-HAM simulation based on an earlier version of ECHAM and HAM) and evaluated them against measurements. They found very large disparities among the models. In Tables 2 and 3 we summarize the global and regional dust budget from AeroCom and from our two simulations. The global emission flux derived by both versions of ECHAM6-HAM2.1 (937 Tg/a in the STD and 931 Tg/a in the NEW simulations) is relatively low in comparison with the median of the AeroCom models (1123 Tg/a) and the International Panel on Climate Change (IPCC) estimate of 1000–4000 Tg/a [*Boucher*, 2013]. As mentioned by *Boucher* [2013] the emission flux of dust particles is highly sensitive to the applied cutoff radius. The cutoff radius in our model is rather small (section 2), which explains the relatively low emission flux. Still, the global annual emission fluxes calculated with ECHAM6-HAM2.1 are in the range of the AeroCom models. The simulated burden (STD: 11.2 Tg and NEW: 12 Tg) fits well in the range covered by the AeroCom models (6.8–29.5 Tg, mean value of 15.8 Tg). The STD and NEW simulations result in similar global emissions but there are large differences over specific regions, namely Australia, Asia, and North America. Even though the emission fluxes for Australia remain within the AeroCom range, the emission fluxes are nearly doubled in the NEW simulation in comparison to STD. This behavior will be discussed in more detail in the next sections.

3.3. In Situ Measurements

In the following we show the comparison between the simulation outputs and in situ measurements. The location of all stations we used for this comparison is shown in Figure S1 in the supporting information.

Table 2. Global Budget for Mineral Dust From the AeroCom Models for the Year 2000 and for ECHAM6-HAM2.1 (Standard and New Version) for the Year 2007

	Emission (Tg/a)	Load (Tg)	Wet Deposition (Tg/a)	Dry Deposition (Tg/a)	Sedimentation (Tg/a)	Lifetime (days)
AeroCom median (range) for 2000	1123 (514–4313)	15.8 (6.8–29.5)	357 (295–1382)	396 (37–2791)	314 (22–2475)	4.6 (1.6–7.1)
ECHAM6-HAM2.1 STD	937	11.2	518	71	361	4.3
ECHAM6-HAM2.1 NEW	931	12	483	76	386	4.7

3.3.1. Surface Concentrations

We compare the simulated 2005–2009 annual average of the dust mass concentration found in the lowest model layer with multiannual surface measurements found at remote marine sites (Courtesy of J. Prospero and D. Savoie, University of Miami). These sites are located far away from, and downwind of, dust sources. This database has been largely used for the evaluation of dust models [e.g., *Stier et al*., 2005; *Huneeus et al*., 2011]. We find a general underestimate of dust mass concentrations (Figure 2), which has already been reported and discussed by *Stier et al*. [2005]. The correlation between measurements and simulation has improved in both our model simulations compared to *Stier et al*. [2005]. We used a model version that is improved upon that of *Stier et al*. [2005] (for a better comparison with Figure 3e in *Stier et al*. [2005], see Figure S2 in the supporting information). In particular, new soil properties in East Asia as implemented by *Cheng et al*. [2008] are used and also the representation of aerosol lifetimes is improved as result of the update from HAM to HAM2 [*Zhang et al*., 2012]. The still existing underestimate of dust mass concentrations is particularly pronounced at low dust concentrations. This behavior is likely related to an overestimate of (wet) deposition during the long-range transport of dust plumes in the version of ECHAM6-HAM, we used in this study. Sensitivity tests (not shown) indicate that the representation of the deposition fluxes is substantially improved with an updated version of the model (ECHAM6-HAM2.2) in which a more physically based scheme for wet deposition has been implemented. Note however that even in our version, the correlation coefficients R of both observed and simulated data, (0.86 and 0.77 for the STD and NEW simulations, respectively) are within the range covered by the AeroCom models [*Huneeus et al*., 2011]. The best model performance is reached for stations located downwind of African and Asian dust sources (blue dots in Figure 2). A comparison between measurements and observations is shown for each station separately in the supporting information (Figure S3). We find that on average the correlation between observations and both simulations are better during winter and spring than during summer and fall. It should be mentioned however that these measurements were taken during the 1980s and 1990s, whereas our simulation period is 2005–2009.

3.3.2. Deposition Fluxes

We use the data set assembled by *Huneeus et al*. [2011] to evaluate our simulated deposition fluxes (Figure 3). The data set includes yearly dust deposition fluxes from 84 sites. *Huneeus et al*. [2011] found that the performance of ECHAM5-HAM in reproducing these measurements is low in comparison to some models, which took part in the AeroCom study. Even though the correlation coefficient from both ECHAM6-HAM2.1 simulations appear to improve upon that of the ECHAM5-HAM used in *Huneeus et al*. [2011], the model's ability to reproduce the deposition fluxes remains relatively low. The correlation coefficient is 0.29 (log scale: 0.88) for simulation STD and 0.25 (log scale: 0.84) in NEW (relative bias: 1.23 (STD), 2.57 (NEW); absolute bias: 12.1 (STD), 11.9 (NEW)). The model is able to capture the deposition fluxes in the remote sides of North Africa relatively well (orange and black points in Figure 3). The model has mainly difficulties to reproduce the fluxes in part of the Southern Ocean (dark blue), Eastern (red), and Western (brown) Pacific, which may be related to the issue with excessive deposition rates during long-range transport as discussed in section 3.3.1.

Table 3. Yearly Emission Fluxes (Tg/a) for Regions as Defined by *Huneeus et al*. [2011, Figure 2][a]

	North Africa	Middle East	Asia	South America	South Africa	Australia	North America
AeroCom median (range)	792 (204–2888)	128 (25.6–531)	137 (27–727)	9.8 (0.2–186)	11.8 (2.9–55.4)	30.7 (9.0–129)	2.0 (1.7–286)
ECHAM6-HAM2 STD	525	94	123	6.9	14.5	63	15.7
ECHAM6-HAM2 NEW	578	97	59	10.4	11.9	98	25.9
Crop and pasture	6.6 (1.1%)	1.8 (1.9%)	17.1 (29%)	2.9 (28%)	2.4 (20%)	19.3 (20%)	20.1 (78%)

[a]Last row: yearly emission fluxes from anthropogenic sources as simulated by simulation new (Global 87.4 Tg/a = 9.4%).

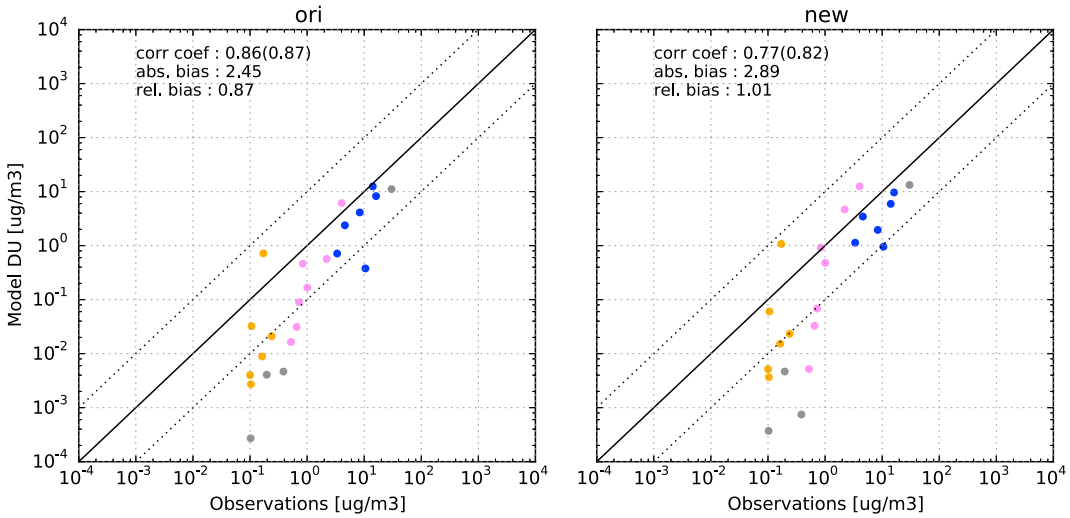

Figure 2. Annually averaged measured surface concentration from the network operated by the University of Miami versus modeled concentrations at each station. The stations are grouped according to *Huneeus et al.* [2011]. They distinguish between remote stations (orange), stations under the influence of minor dust sources of the Southern Hemisphere or remote sites in the Northern Hemisphere (violet), and locations downwind of African and Asian dust sources (blue). Correlation coefficient and absolute and relative biases are indicated for both simulations. The correlation in respect to the logarithm of the model and of the observation is given in parentheses.

We also compare our results with dust deposition rates measured between 1994–1996 at three representative sites selected by *Huneeus et al.* [2011] from the Florida Atmospheric Mercury Study (FAMS) network [*Prospero et al.*, 2010] (Figure 4). It should be noted that two of the stations, namely, Tamiami Trail and Little Crawl Key, that present rather different wet deposition rates, are located within the same grid box in our model simulation.

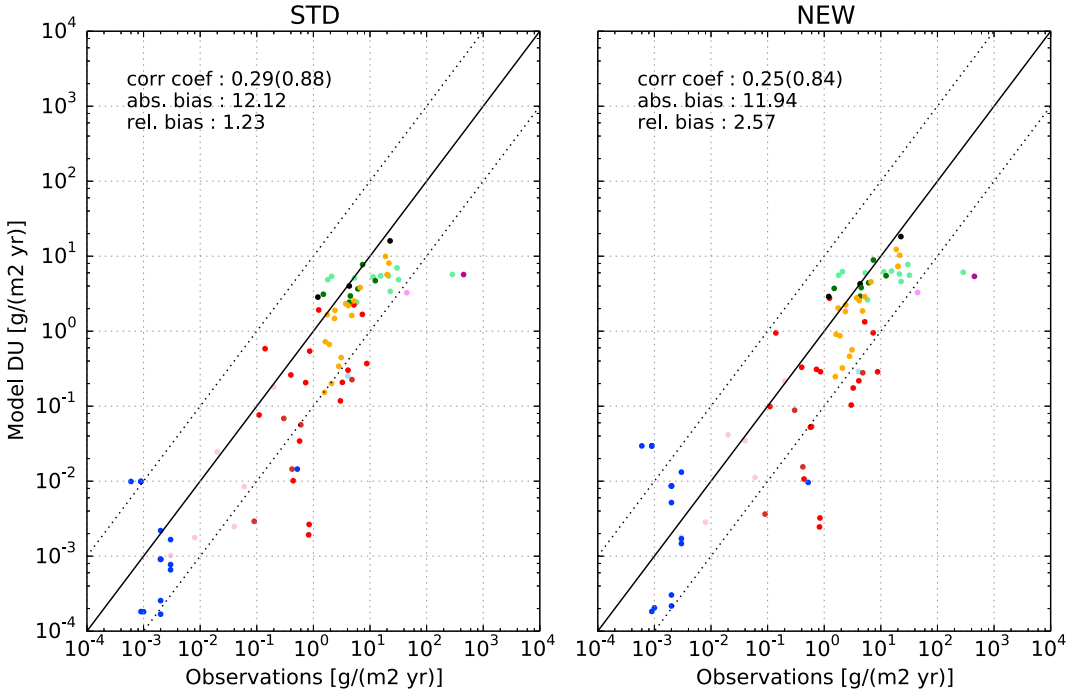

Figure 3. Measured annual dust deposition fluxes versus modeled ones; units are g m^{-2} yr^{-1} . Points are colored regionally for West/East Pacific (red/brown), North/Tropical/South Atlantic (orange/black/light blue), Middle East/Asia/Europe (violet/purple/light green), Indian/Southern Ocean (dark green/dark blue) and ice core data in Greenland, South America, and Antarctica (pink). The data are taken from *Huneeus et al.* [2011].

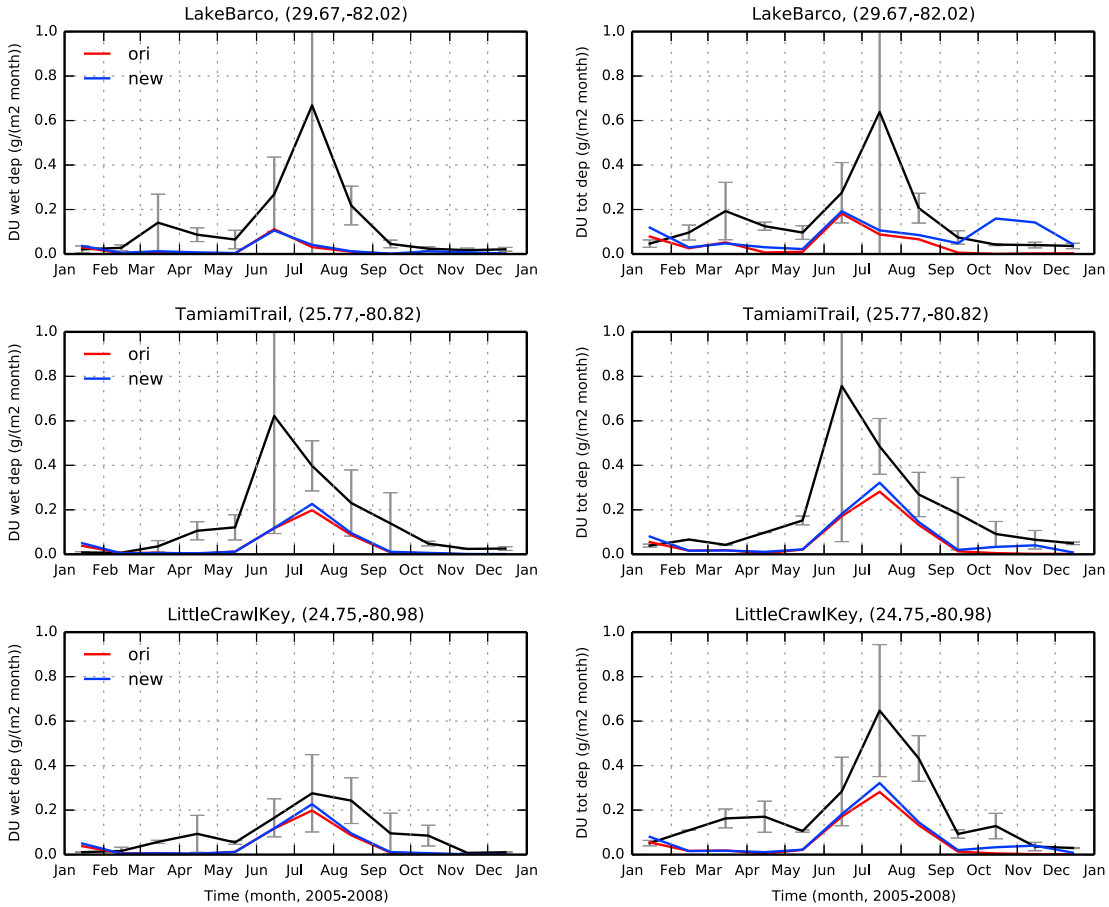

Figure 4. (left) Observed and modeled wet and (right) total dust deposition rates at three sites from the Florida Atmospheric Mercury Study (FAMS) network. The black line is the mean of the 3 years of FAMS data from 1994 to 1996. Vertical lines correspond to one standard deviation of the 3 year average. Note that the stations Little Crawl Key and Tamiami Trail are located in the same grid box in our model simulations.

This illustrates the variability within one model grid box and the difficulty for a global model to reproduce point measurements. Nevertheless, this comparison indicates that our model systematically underestimates the magnitude of the deposition fluxes, even though it captures rather well the seasonality (maximum in summer) and the dominance of wet deposition in summer.

3.3.3. AERONET Stations

We further used the Aerosol Robotic Network (AERONET) stations [*Holben et al.*, 1998, 2001] to compare measured and simulated Aerosol Optical Depth (AOD) at 500 nm. We focus on stations, which are more largely influenced by mineral dust particles. Both STD and NEW simulations agree reasonably with the observed AOD (Figure 5; temporal correlation of all stations with simulation STD/NEW: $R = 0.67/0.61$; absolute bias: 0.174/0.172; relative bias: 0.335/0.335) indicating that our new approach has not degraded (though not improved either) the dust simulation. Measurements at stations located in America (blue) are well captured by the model. The measurements taken at African stations (orange) are relatively well reproduced by the simulations. But there is a clear underestimate in AOD in stations located in Middle East, as previously noted by *Huneeus et al.* [2011] for the ECHAM-HAM model. The similarity between the STD and NEW simulations is also pronounced in Figure 6, where the monthly evolution of simulated and measured AOD is shown for specific stations. At most of the stations both simulations capture the seasonal variations quite well but they underestimate the peak in AOD during summer. Exceptions are Dakar and Capo Verde, where both simulations overestimate the maximum AOD.

3.4. Satellite Measurements

3.4.1. Large-Scale AOD Pattern

We next investigate the ability of our model to simulate large-scale dust patterns by comparing with observed Aerosol Optical Depth (AOD) at 550 nm provided by different satellite retrievals (Figures 7 and S4). It

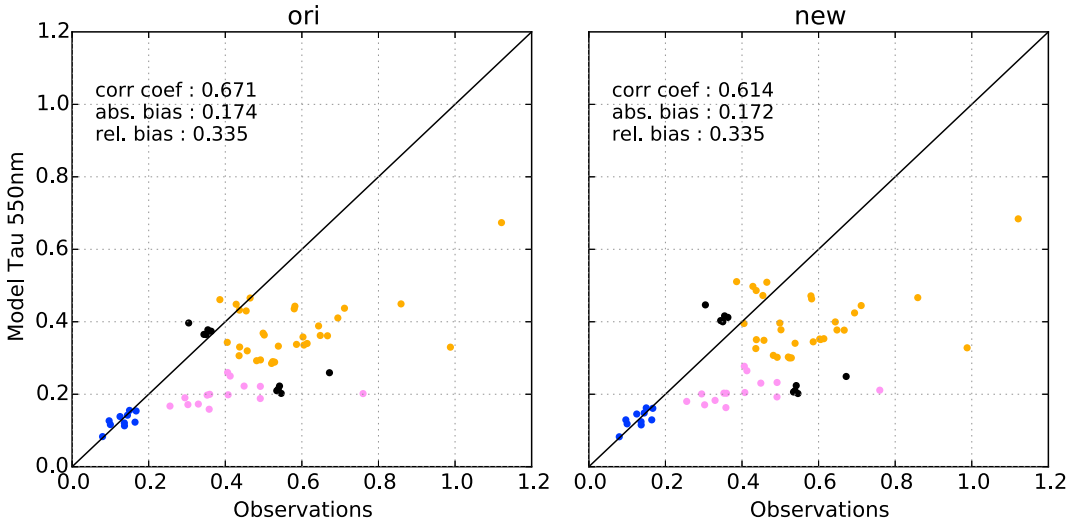

Figure 5. Annual averaged AOD at 550 nm measured at dusty sites of the AERONET network stations (as selected by *Huneeus et al.* [2011]) versus simulated AOD (left simulation: STD, right: NEW). Shown are results for the time period January 2005 until December 2009 (if measurements are available). The stations are regionally grouped into African (orange), Middle East (violet), American (blue), and stations elsewhere (black).

should be noted that we compare here simulation data averaged over time intervals of months with monthly averages of satellite measurements obtained at specific overpass times. In addition, even though we focus our comparison on regions more strongly impacted by dust, differences between simulated and observed AOD may also be attributable to other aerosol components.

Figure S4 in the supporting information shows observed AOD from different instruments (namely: CALIOP, Cloud Aerosol Lidar with Orthogonal Polarization [*Hunt et al.*, 2009]; MISR, Multiangle Imaging Spectroradiometer instrument [*Diner et al.*, 2001]; MODIS, Moderate Resolution Imaging Spectroradiometer [*King et al.*, 1992, 2003]; MODIS Deep Blue—special algorithm which expands the coverage of the MODIS instrument over bright surfaces [*Hsu et al.*, 2004]) in comparison with AOD simulated in the STD and NEW simulations for March 2007. March is a very prominent month for dust outbreaks in Africa. Both simulations agree well with the satellite products in this region as well as in most regions of the so-called Dust Belt. In Western United States the model underestimates AOD. Recent studies comparing MODIS land retrievals and AERONET observations indicated that MODIS AOD is high relative to AERONET for this region, which is attributed to poorly characterized retrievals over marginally bright surfaces [*Drury et al.*, 2008; *Levy et al.*, 2010]. This high bias in the MODIS AOD may thus explain the better agreement of the model with MISR and CALIOP in these regions.

3.4.2. Time Series

A better insight into the performance of our model can be obtained when focusing on regions known to be strong dust emitters. The temporal evolution of simulated AOD and those obtained from the satellite products for North Africa, Middle East, Asia, and Australia is shown in Figure 7. In general, the differences of the different satellite estimates of AOD are quite large for these regions.

For North Africa, the world's largest dust source region, both simulations are able to reproduce the measurements adequately. Only during fall the model seems to underestimate the AOD. Both model simulations underestimate AOD in the Middle East. These results are consistent with the comparison between in situ measurements (section 3.3). For Asia, there is also a general underestimate in simulated AOD. While both simulations give similar values for AOD, they produce quite different dust emissions (Table 3) but none of them substantially improve the overall comparison with AOD. This may result from an underestimate of the contribution of anthropogenic aerosols, which is large over this region.

While the results for AOD are quite similar in both of our simulations for all the regions considered so far, they differ substantially for Australia throughout the 3 years. The simulation NEW appears to predict (and in some cases overestimate) some peaks in AOD in austral summer. This is likely due to the distribution of natural vegetation from *Ramankutty and Foley* [1999] used in JSBACH, which assumes that large parts of Australia are

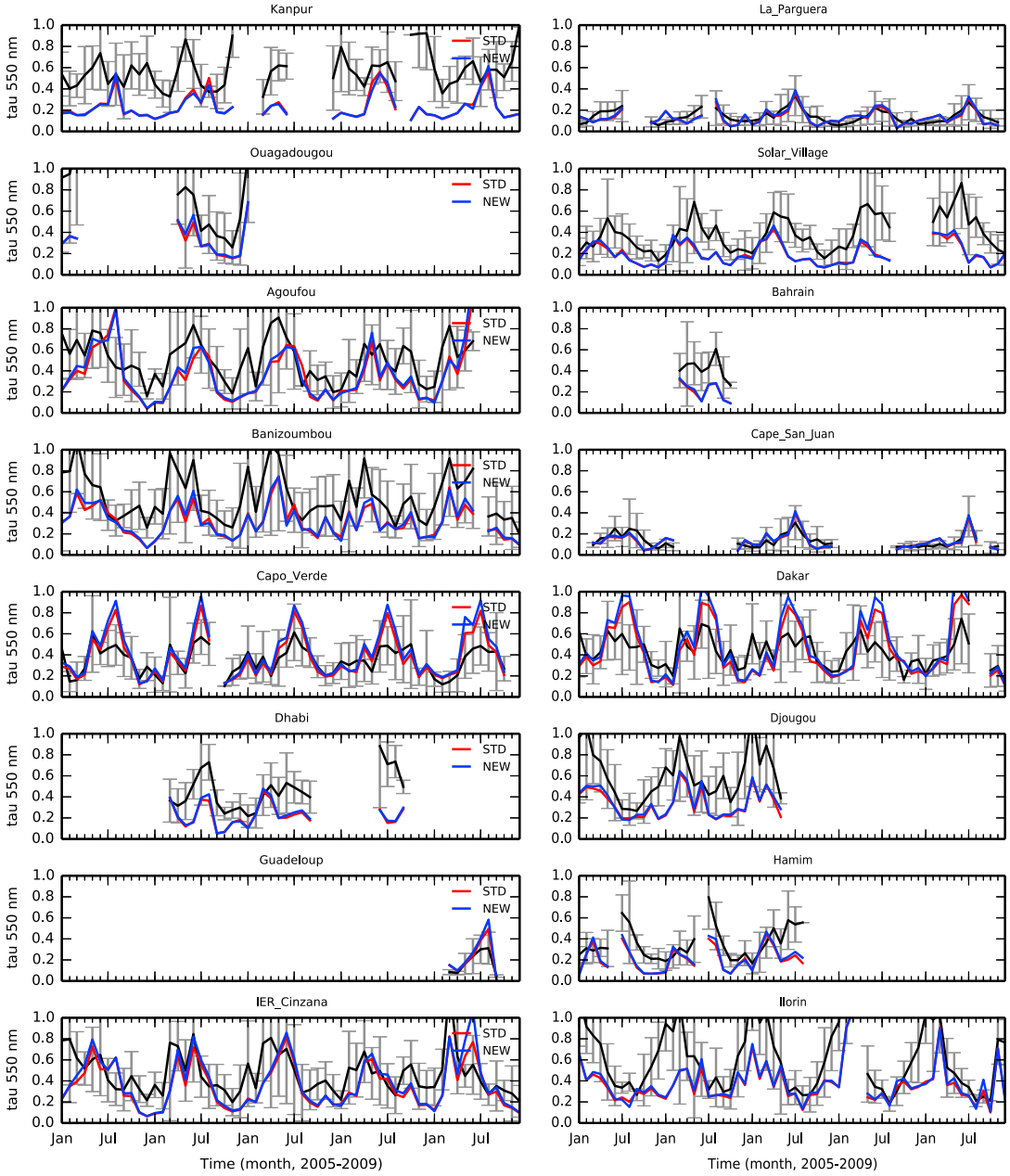

Figure 6. Temporal evolution of monthly mean AOD as measured by AERONET sides (black) and simulated with STD (red) and NEW (blue) for different locations. The bars refer to the monthly variations of the measurements.

covered with grasslands (instead of shrublands which could be more realistic). This, in turn, results, in relatively large areas, which can potentially act as dust source. This behavior of the simulation NEW should be kept in mind when interpreting the results of section 4.

3.4.3. Dust Optical Depth

Ginoux et al. [2012] retrieved Dust Optical Depth (DOD) from MODIS Deep Blue satellite measurements for the time period 2003–2009. Following their study, we calculated the number of days per season with DOD $>$ 0.2 using our simulation output for the time period 2005–2009 (Figure S5 in the supporting information). In accordance to the results presented before, the frequency of days with DOD $>$ 0.2 calculated from both model simulations are quite similar. The highest frequency of dust days occurs in North Africa during spring and summer in both observations [*Ginoux et al.*, 2012] (Figure 5) and simulations. The seasonality reported by

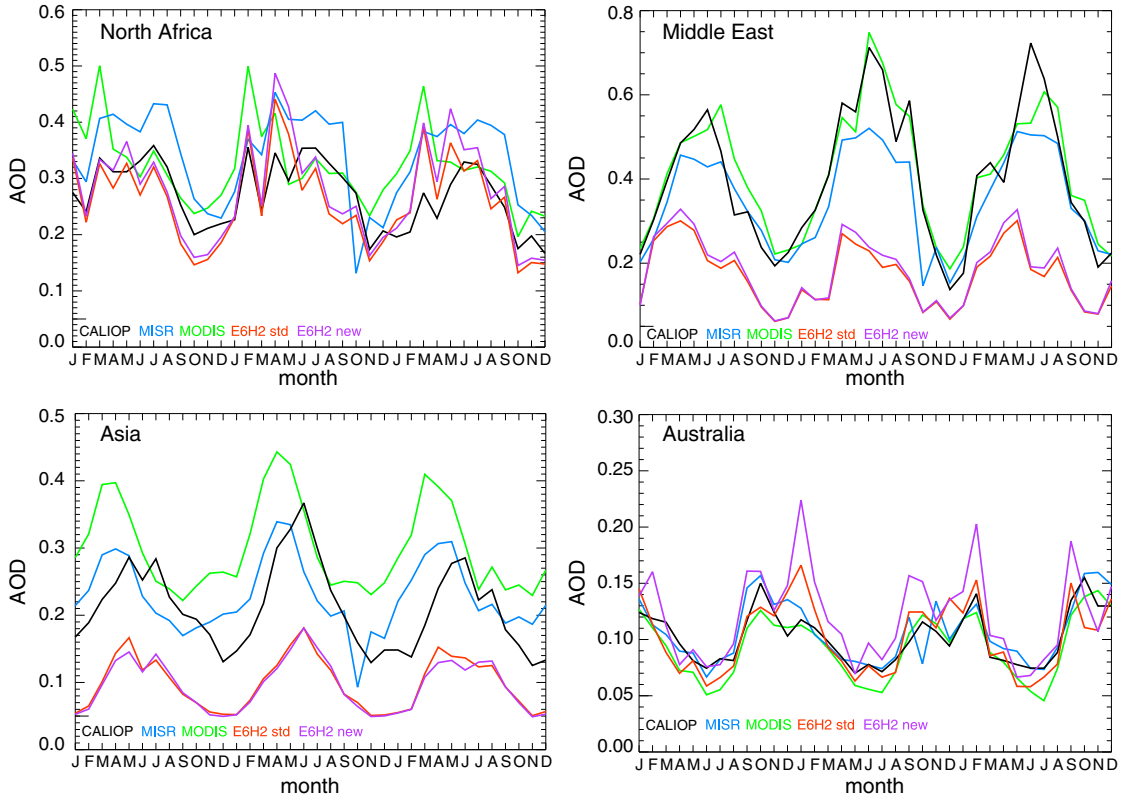

Figure 7. Temporal evolution of monthly means of measured (black, blue, and green lines) and simulated (red and purple lines) AOD at a given region for time period January 2005 until December 2009 (note that scales differ between regions).

Ginoux et al. [2012] with a maximum in spring and summer (March–May and June–August in Northern, and September–November and December–February in Southern Hemisphere) is also well reproduced by our simulations. A remarkable difference between observations and simulations (especially NEW) is the occurrence of days with DOD $>$ 0.2 in the western part of Australia. Another one is the underestimation of the frequency in the U.S. and Northern India, especially during spring.

3.5. Conclusion of the Model Evaluation

In conclusion, the evaluation shows that the new algorithm developed to estimate potential dust source areas together with the ECHAM6-HAM2 model yields results of similar quality than the original algorithm by *Tegen et al*. [2002] for present time. We should acknowledge that we are not able to test if the emission fluxes from agricultural areas are better represented in the modified routine than in the original one. However, as we assume that historically farmers established pastures preferentially on natural grasslands rather than on other vegetation types (see section 5 and also *Reick et al*. [2013]) and that natural grasslands are handled in the same way as pasture, we do not expect large differences between the original and the new algorithm in the pasture-dominated regions (like wide parts of Sahel).

Our dust simulations however still suffer from some deficiencies. In particular, the model underestimates the dust concentrations in some source regions, e.g., Asia, Middle East, and the US. This behavior could be caused by the coarse resolution of our global model (approximately 200 km $\times$ 200 km). With such a coarse resolution small-scale processes are not resolved explicitly. Therefore, peaks in wind velocity caused by small-scale processes cannot be reproduced by the model (see also the discussion in section 4). To account for this fact the threshold of the friction velocity, which has to be reached to allow dust emissions, is lowered by a global constant correction factor (section 2.1). Since the model is somehow tuned to reproduce the dust burden in the main source regions (North Africa), this value could be unrealistic for other regions of the world. Maybe the models capability to represent dust emissions in the Middle East or Asia could be improved by introducing corrections factors depending on source regions. Dust maybe overestimated over Australia in the NEW simulation.

Table 4. Emission Fluxes From Our Four Base Simulations (See Table 1) Before Slash: 10 Year Mean Annual Total Emission Fluxes and Standard Derivation (Tg/a)[a]

	Global	North Africa	Middle East	Asia	South America	South Africa	Australia	North America
pCpL	912 ± 77/90 ± 8	491 ± 66/8 ± 1.6	111 ± 11/4 ± 0.4	57 ± 12/13 ± 3.3	11 ± 3.6/3.5 ± 1.2	7 ± 1.9/2 ± 0.6	156 ± 28/27 ± 5	27 ± 7/18 ± 5
hChL	729 ± 75/18 ± 3	417 ± 56/3 ± 0.7	107 ± 15/1 ± 0.1	48 ± 8/3 ± 0.7	6 ± 1/0.3 ± 0.05	5 ± 1/0.3 ± 0.1	90 ± 21/3 ± 0.6	17 ± 5/4 ± 1.6
pChL	832 ± 90/20 ± 4	495 ± 82/3 ± 0.6	113 ± 16/1 ± 0.1	49 ± 5/3 ± 0.5	8 ± 2.4/0.4 ± 0.2	7 ± 1.4/0.5 ± 0.1	97 ± 23/3 ± 0.7	20 ± 6/5 ± 2.8
hCpL	801 ± 39/72 ± 9	428 ± 31/7 ± 1.5	112 ± 17/3 ± 0.5	51 ± 8/11 ± 2	7 ± 1.9/2 ± 0.6	7 ± 1.5/2 ± 0.5	131 ± 29/22 ± 4	20 ± 5/11 ± 4

[a]After slash: 10 year mean annual emission fluxes from agricultural sources for regions as defined by *Huneeus et al*. [2011, Figure 2]. The numbers do not exactly add up because of nonlinearity in the system.

Dust deposition fluxes far away from sources are largely underestimated, which likely results from a problem with the wet deposition rates, rather than the dust sources. Despite these problems, which should be kept in mind when interpreting the results presented in the next section, we conclude that we are able to reproduce the dust load in such a way that we can use the modified model system to address our research question.

4. Changes in Dust Emissions and Associated Radiative Forcing Between the Late 19th and Early 21st Century

Using the new method for deriving potential dust source regions consistently from the ruling climate conditions and land cover, we are now able to investigate the relative impact of ALCC and CC on dust burden changes and associated radiative forcing, focusing on the 20th century.

4.1. Global Results

Overall, we obtain similar global annual mean emissions for the decade 2000–2010 (simulation pCpL) as in simulations NEW and STD discussed above (see Tables 2 and 4).

About 730 Tg/a of dust particles are emitted globally in the late nineteenth century (hChL, Table 4 and Figures 8 and 9). Only 2.5% of these emissions take place in agricultural areas. We find that dust emissions increased by 25% during the twentieth century, reaching 912 Tg/a at present time. Changes in land cover (mostly conversions of areas with natural vegetation into agricultural lands) contribute to about 40%, while climate change contributes to about 60% to these changes. For present condition, we find that about 10% of dust emissions are due to agricultural areas. This finding is in good agreement with *Tegen et al*. [2004] but lower than the value recently reported by *Ginoux et al*. [2012], who found that 20% of dust emissions are from vegetated surface (mainly agricultural areas). Note that the lifetime of dust particles remains quite similar between the two periods we investigated (4.36 days (dry: 9.03 days; wet: 8.44 days) in present conditions and 4.38 days (dry: 9.31 days; wet: 8.25 days) in historical times).

We find a global dust burden of 8.78 Tg in the late nineteenth century, which increases by 24.5% to reach 11 Tg (Table 5) for today's conditions. The resulting change in radiative forcing is $-0.14\,W/m^2$, in good agreement with the results of *Mahowald et al*. [2010] (though they also reported large decadal variability) and the values published in the latest IPCC report of -0.10 (-0.3 to $+0.1$) W/m^2 [*Boucher*, 2013]. IPCC estimates of the direct forcing of anthropogenic aerosols are $-0.35 \pm 0.5\,W/m^2$ [*Boucher*, 2013], indicating that changes in dust emissions due to humans should not be neglected. Taken individually, the effect of CC and ALCC result in a decrease in negative forcing of $0.08\,W/m^2$ and 0.05, respectively.

To capture the influence of dust changes on the indirect aerosol effect is quite difficult. We note however that changes in all sky forcing (which includes modifications in cloud cover due to changes in dust concentrations) are quite similar to the differences in clear-sky forcing ($-0.11\,W/m^2$).

Historical changes in dust emissions and the respective reasons for these changes vary from one region to another (Figure 8). In the next paragraph we focus on the most important dust source regions (North Africa and Asia) and two regions, which are subject to large anthropogenic land cover changes, namely, North America and Australia.

4.2. North Africa

The largest dust source region in the world is North Africa [e.g., *Engelstaedter et al*., 2006]. During the 1880s, 417 Tg of dust are emitted annually; therefrom, only 2.8 Tg/a are emitted from agricultural sources (Table 4 and Figure 9). The emission flux increases to 491 Tg/a (+18%) between 1880 and today mainly due to an

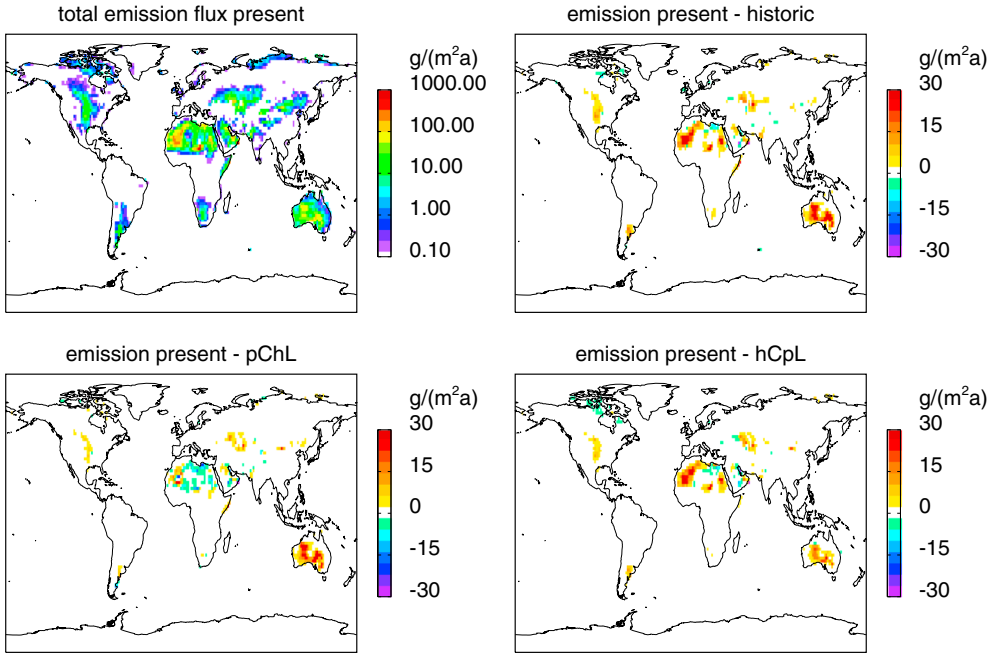

Figure 8. Ten year mean annual dust emission flux as simulated in (top left) present (pCpL), (top right) differences between simulation pCpL and past (hChL), (bottom left) pCpL and present climate historic land use (pChL), and (bottom right) pCpL and historic climate and present land use (hCpL).

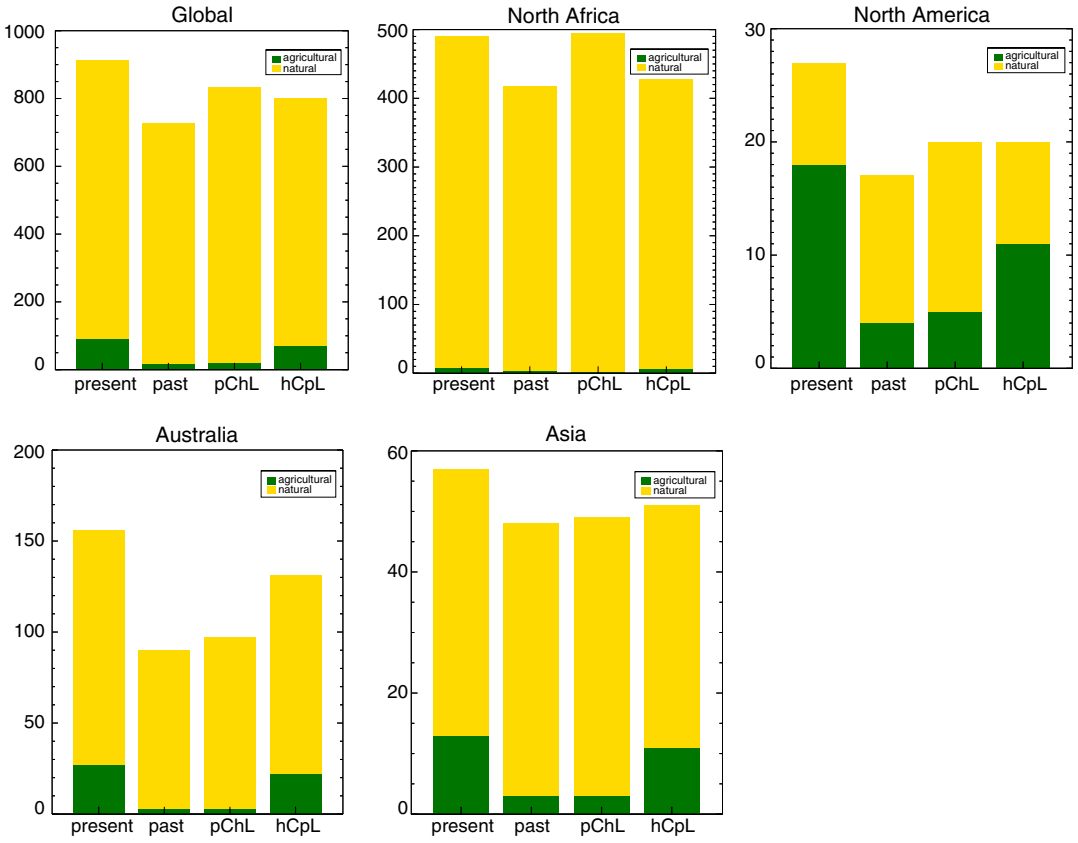

Figure 9. Integrated 10 year mean annual dust emission flux in Tg/a for different regions as simulated in simulation present, past, pChL (present climate historical land use), and hCpL (historical climate present land use). Dark green denotes emissions from agricultural source regions and yellow emissions from natural source regions. Note the use of different axis ranges.

Table 5. Change in Dust Burden Between Simulation *x* and hChL (((*x*-hChL)/hChL)*100) for the Same Regions as in Table 4

	pCpL < − > hChL	pChL < − > hChL	hCpL < − > hChL
Global	24.5%	16.6%	6.9%
North Africa	15.9%	19.4%	−0.5%
North America	41.4%	22.3%	24.7%
Australia	71.1%	7.2%	43.2%
Asia	13.6%	4.9%	4.9%
Middle East	8.8%	9.8%	4.5%

increase in wind speeds induced by CC (Figure S8 in the supporting information). For today's conditions, we find that 8 Tg/a of dust are emitted from agricultural areas and mostly take place in Sahel (Figure S6). This is in a good qualitative agreement with the results of *Ginoux et al.* [2012] (Figure 7). We also find that agricultural areas (crop and pasture) contribute by 1.6% to the total emission flux over the region. This is consistent with the value of *Ginoux et al.* [2012] who reported that 4% of the total emissions come from vegetated areas, which include crop, pasture, as well as natural areas in their study.

If we consider historical land cover in present climate, the emission flux is slightly higher than in our present-day simulation (495 Tg/a). The reasons are a decrease in precipitation in Sahel (Figure S7) and an increase in wind speed (Figure S8) due to biogeophysical feedbacks (e.g., changes in near-surface energy, moisture, and momentum fluxes induced by large-scale changes in land cover). In our model, dust emissions can only take place if the skin reservoir is nearly empty. After rainfall the skin reservoir is filled and no dust emission can take place. Thus, a decrease in precipitation results in an increase in dust emissions. In addition, deforestation in the Sahel causes a decrease in roughness length, which results in an increase in wind speed. Since dust emissions are very sensitive to changes in wind speed, the emission of dust particles increases.

Mulitza et al. [2010] constructed a 3200 year record of dust deposition off northwest Africa (station GeoB9501; 16°50'N, 16°44'W). They found a sharp increase in dust deposition at the beginning of the nineteenth century. Using their data (supporting information, Table 8, median Aeolian flux), we computed an increase of 167% in deposition fluxes between the 1880s (mean 1880.7–1889.0) and the 2000s (1999.4–2005.6). We also find an increase in the simulated dust deposition flux for this site but only of 36%. *Mulitza et al.* [2010] report that a large fraction of the dust transported to the site is constituted of coarse particles, which we do not reproduce well in our model (section 2). It should be noted that *Mulitza et al.*'s [2010] findings do not seem to be fully consistent with those of *Mahowald et al.* [2010], who reported low changes in dust emissions over a similar period but pointed out a large decadal variability with a well-marked increase in dust sources between a "low dusty" period (1955–1964) and a "more dusty" period (1980–1989). *Mulitza et al.* [2010] also reported that the increase in dust deposition flux results from an increase in emission fluxes in North Africa associated with the onset of commercial agriculture in the Sahel region. This is consistent with our finding that ALCC is an important factor, though CC plays the dominant role in this specific region.

In our model, as a result of the emissions increase, the dust burden increases by 15.9% (from 4 to 4.6 Tg, Table 5) between historical times and present day. This, in turn, results in a change of clear-sky radiative forcing at top of atmosphere (TOA) of -0.6 W/m^2. Locally, the change in forcing is up to -3 W/m^2 (Figure 10).

4.3. North America

In the 1880s, 16.8 Tg/a of dust particles are emitted in North America, with only 4.1 Tg/a arising from agricultural areas. For present conditions the North American mean dust flux increases to 26.7 Tg/a (+59%) with 17.7 Tg/a (66%) being emitted from agricultural source regions. The simulated contribution of emissions from agricultural source regions to the total emission flux agrees well with the estimates of *Ginoux et al.* [2012], who derived a contribution of all vegetated areas of 78%.

The simulated increase between past and present emission flux (Figure 9) is caused by both CC and ALCC. The area of potential dust sources increases due to land cover change as well as to a decrease in precipitation. The decrease in precipitation is caused by the changes in climate itself (simulation hCpL) but also by changes in land cover via the biogeophysical feedbacks (as seen in the simulation pChL).

Based on our model evaluation presented in section 3, we know that the model tends to underestimate the dust load in North America. Nevertheless, the distribution of anthropogenic dust sources (Figure S5) is quite

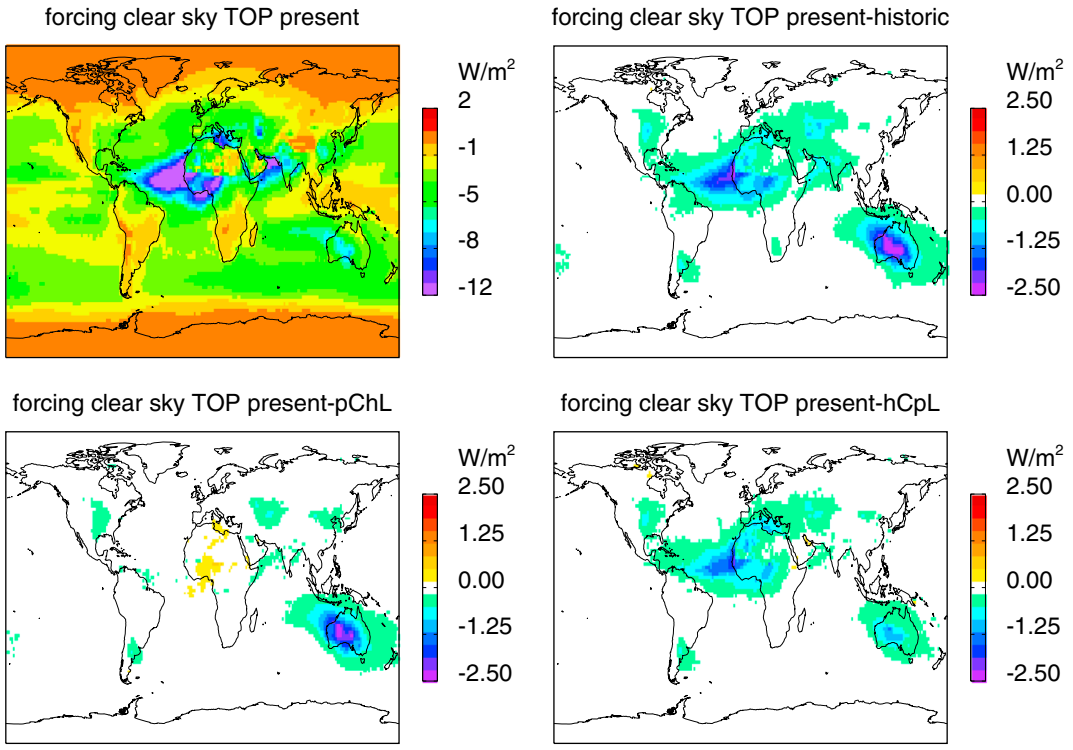

Figure 10. Ten year mean clear-sky radiative forcing due to aerosols at TOA for the (top left) simulation present (pCpL), (top right) differences between simulation pCpL and past (hChL), (bottom left) pCpL and present climate historic land use (pChL), and (bottom right) pCpL and historic climate and present land use (hCpL).

comparable with the findings of *Ginoux et al.* [2012]. Especially, the regions of the High Plains and Big Sioux River are well reproduced by our model.

We further compare our results with those from *Neff et al.* [2008] who used accumulation rates of alpine sediments at three sites located in southwestern Colorado downwind of the major western U.S. deserts to discuss changes in sources. They reported a decrease in dust deposition during the twentieth century [*Neff et al.*, 2008, Figure 1], and based on the same data *Mahowald et al.* [2010] derived decreasing dust sources over North America over the twentieth century. Figure 11 shows the simulated changes in dust deposition fluxes between the 1880s and the 2000s. In the vicinity of the region where *Neff et al.* [2008] collected data, our model simulates a rather sharp spatial gradient in dust deposition changes, with a decrease in deposition flux in the western U.S. and a rather large increase over Central and eastern U.S., which makes the comparison with the point measurement difficult. Overall, we find that the North American dust emissions increase over our study period (Figures 8 and 9), even though some regions show negative changes in dust deposition. *Neff et al.* [2008] indicated that increased dust deposition in the early twentieth century is related to land use change, in particular the expansion of livestock grazing. This appears to be consistent with our results about the importance of ALCC.

As a result of our increasing emissions, the dust burden increases from 0.21 Tg to 0.30 Tg (+41.4%, Table 5) between the 1880s and the 2000s. This results locally in a change of up to -1 W/m^2 in clear-sky radiative forcing at top of atmosphere (TOA). For present-day conditions, the regional averaged clear-sky forcing at TOA is -2.15 W/m^2. The change in radiative forcing across the twentieth century is 0.06 W/m^2. This change in forcing is caused by both ALCC and CC, but CC is the most important driver. Since nearly 70% of dust particles are emitted from agricultural sources in North America, land cover changes have to be taken into account when investigating changes in dust emissions associated with climate change and air quality issues.

4.4. Australia

We simulate an annual averaged dust emission flux of 89.8 Tg/a (with 2.8 Tg/a emitted from agricultural areas) for the late nineteenth century conditions, which increases to 156.1 Tg/a for today (with 27 Tg/a or 17%

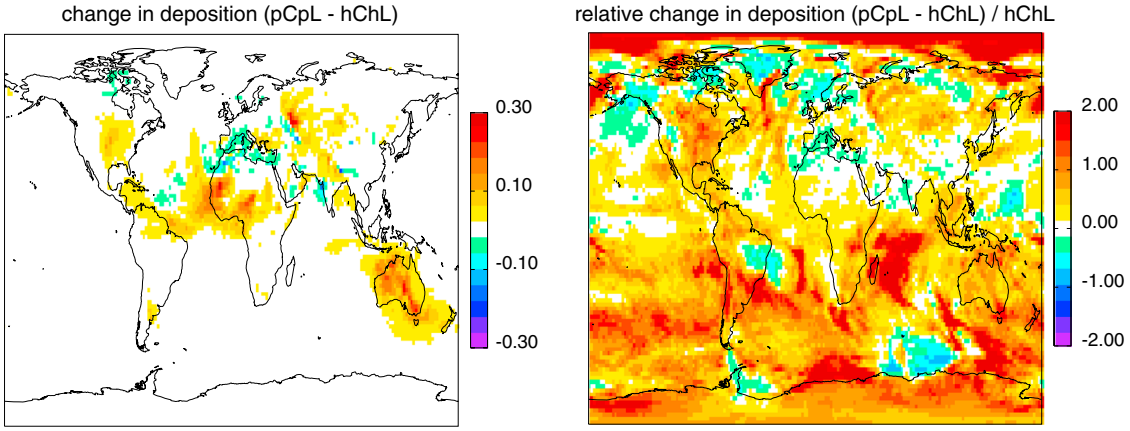

Figure 11. Total (unit is kg/(m^2 s), left) and relative (right) changes in 10 year mean deposition fluxes between simulation present and past.

being emitted from agricultural sources). This value of 17% is lower than the value of 38% reported by *Ginoux et al*. [2012]. However, again, the comparison is difficult since *Ginoux et al*. [2012] include all types of vegetation (and not only anthropogenic ones) in their category.

Our model sensitivity simulations indicate that the large increase in emission fluxes between the 1880s and the 2000s is caused by both ALCC and CC, with ALCC being the main driver (Figures 8 and 9 and Tables 4 and 5). The transition from natural vegetation to agricultural cover causes a decrease in roughness length, which modifies the circulation and results in an increase in 10 m wind speed (Figure S8). In addition, the direct effect of transformation of natural vegetation into agricultural land results in an increase in emissions, as shown by the increase of 24 Tg/a in dust flux from agricultural areas.

Mahowald et al. [2010] estimated the variability in dust source strength in Australia mainly based on dust deposition fluxes derived from ice cores in Antarctica. They found relative small changes but reported large decadal variability. Our model simulates an increase in dust deposition throughout Australia, though some regions over the Antarctic Ocean show a decrease (Figure 11). Even though we have to acknowledge that our model has some difficulty to reproduce aerosol long-range transport, this result indicates that changes in dust emissions inferred from regional changes in dust deposition may be subject to large uncertainties. Note also that we find large differences in dust emissions between our nudged (90 Tg/a) and free running (158 Tg/a) simulations, the latter being outside of the range reported in *Huneeus et al*. [2011]. For this reason, our results for Australia should be interpreted with caution.

The change in dust emissions results in an increase in dust burden from 0.76 Tg to 1.3 Tg during the twentieth century (pCpL versus hChL), which corresponds to an increase of 71.1% (Table 5). For Australia the average TOA clear-sky forcing of dust aerosols is -4.21 W/m^2 in present conditions. The twentieth century change of -0.87 W/m^2 is mainly caused by ALCC.

4.5. Asia

We simulate a dust emission flux of 48.1 and 57.1 Tg/a for the 1880s and 2000s, respectively. The contribution of agricultural source regions is estimated to be 23% for present day. Our simulated regions with large anthropogenic dust sources (Figure S5) for India and also for some regions in China (e.g., the North China Plains) are qualitatively consistent with *Ginoux et al*. [2012].

Mahowald et al. [2010] reported relatively small changes between the beginning and the end of their study period but large temporal variability in dust deposition and thus source strength. Our model simulates a large spatial variability in dust deposition flux changes throughout Asia, with positive values in Central Asia and close to zero or negative values over large part of India and China (Figure 11). Our mean dust emissions increase by about 20% between the 1880s and 2000s but this increase is largely restricted to a specific region, in particular over Central Asia (in the area of the Balkhash depression, in the region border of Kazakhstan and Russia,). There we find that the dust emission flux increases due to a decrease in precipitation (Figure S7), which is caused mainly by CC but also by ALCC via biogeophysical feedbacks. The *Hurtt et al*. [2011] data used

for our simulations show substantial changes in land use in this region (noted by *Ginoux et al*. [2012] as a region with rather large anthropogenic influence), which results in changes in emissions. The region of the North China Plains also experienced changes in land use with some implications for emissions. Overall, the simulated increase in dust emissions from 1880 and today is driven by both ALCC and CC.

Dust burden increases from 0.81 Tg to 0.92 Tg (+16.6%, Table 5) between 1880 and today. The resulting average change in clear-sky radiative forcing at TOA is -0.1 W/m^2 and as large as 1 W/m^2 locally.

4.6. Discussion

The model evaluation presented in section 3 has shown that our model has some limitations in reproducing measurements in an adequate manner. The model has especially a problem with long-range transport (this point will be corrected in the upcoming version of the model, ECHAM6-HAM2.2). But focusing on changes in dust emission and burden close to source regions the influence of that deficiency on the results should be rather small.

We use a global climate-aerosol model for our study. In general, the horizontal resolution of a global model system is necessarily rather course (e.g., we performed our study in T63 horizontal resolution, approximately 200 km $\times$ 200 km). Models with such a coarse resolution can resolve synoptic systems but are unable to resolve smaller scale systems (e.g., convective systems). Therefore, our model is not able to simulate dust emissions due to cold pool outflows from moist convection ("haboobs") or microscale dust devils. The estimated contribution from haboobs to the total dust emission flux differs between regions. In Australia the contribution is with only 9% [*Strong et al*., 2011] rather small. But in areas affected by the West African monsoon, the influence of haboobs can reach up to 67% [*Bou Karam et al*., 2009]. Due to changes in climate and/or land properties, the number and strength of haboobs may have changed.

Additionally, our results are affected by inherent assumptions underlying our modeling system. For example, we assume that farmers protect their ground against erosion in the same manner all over the world. But in reality, there are quite some differences in soil conservation practices between regions. *Ginoux et al*. [2012] have pointed out the sensitivity of derived dust fluxes to the applied threshold of the friction velocity. Since we increased the friction velocity in crop fields by 40% all over the world, this assumption is quite crucial for our derived emission fluxes. In addition, it is questionable whether farmers in the past applied the same soil conversion techniques than today. To test the importance of this latter assumption, we performed an additional sensitivity simulation. In that simulation (not shown), we did not increase the threshold of the friction velocity in crop fields for historical conditions. We find that historical global emissions change by less than 0.1%, indicating that this assumption has no impact on our results regarding the relative contribution of CC and ALCC.

Further, we assume that the soil particle size distribution and the soil properties are the same in agricultural and natural soils, which may result in an overestimate of the amount of small dust particles, emitted from agricultural source regions.

In our setup, strong assumptions are made for the radiative properties of dust. For example, we neglect emissions of large particles. But the longwave radiation is in particular affected by the existence of large particles in the atmosphere. These particles are found mostly at or close to dust source areas [*Ryder et al*., 2013]. Therefore, we may underestimate the contribution of the longwave radiation to the total radiative forcing in source regions. Since source regions change over time (due to ALCC), this could slightly affect our estimated change in radiative forcing. In addition, *Kok* [2011] suggested that the size distribution of naturally emitted dust aerosols might be independent of wind speed, contrary to what we assumed in HAM. Furthermore, we apply the same mineralogical composition to all dust particles, independent of their source regions.

Our results on dust emissions are supposedly also affected by a peculiarity of the implementation of the transition between natural and agricultural lands in JSBACH. It is assumed that historically farmers established pastures preferentially on natural grasslands rather than on other vegetation types (such as forests) [*Reick et al*., 2013]. ALCC thus results in our model in a conservation of forested areas and subsequently lower changes in dust emissions than without this assumption. This should mostly affect emissions in regions with former mixed forest/grass vegetation. In addition, our estimate of potential source areas per grid cell strongly depends on the applied vegetation map. *Jung et al*. [2006] discussed the difficulties encountered when deriving vegetation maps and the resulting differences in vegetation maps. Another source of bias may be the "translation" of the maps for agricultural lands onto a global model grid as discussed in the intercomparison study by *de Noblet-Ducoudré et al*. [2012].

5. Summary and Conclusion

In this work, a new approach is proposed, which allows deriving potential source regions within the climate-aerosol model ECHAM6-HAM2 prognostically. In particular, the geographic location of dust sources is not prescribed from satellite observations (as in the standard version of ECHAM6-HAM2) but computed interactively from the land cover state provided by the land component JSBACH. We evaluate our model against satellite data and surface measurements and compare our results with other global dust models. We find that our global emission fluxes are low in comparison to most other global models but still in the range reported by *Huneeus et al.* [2011]. The relatively small emission flux is partly caused by the small cutoff radius (section 2) applied for dust emissions in HAM2. The dust simulation in both the standard model version and with use of our new approach underestimates observed concentrations to some extent in some source regions, e.g., Middle East and the U.S. The dust load in the large source region of North Africa is reproduced adequately. Observed AOD is also underestimated over Asia but it is difficult to dismantle whether this is due to too low dust emissions or too low anthropogenic aerosol emissions. Overall, the dust deposition fluxes far away from sources are too low, a problem likely due to inaccurate deposition rate during long-range transport (this issue will be improved to some extent in upcoming versions of the model). Both the STD and the NEW simulations result in relatively similar dust budgets, although dust load may be overestimated over Australia by the new approach.

Our new approach allows us to distinguish between natural and anthropogenic (i.e., agricultural) dust emissions. Overall, we find a good qualitative agreement between the contributions due to agricultural areas derived by *Ginoux et al.* [2012] and in our model.

We next investigated the change in dust concentrations between the late 19th and the beginning of the 21st century, as well as the relative role of climate change and anthropogenic land cover changes. Over this period, annual dust emission fluxes increased globally from 729 Tg/a in the 1880s to 912 Tg/a in the 2000s decade. Based on our simulations, both CC and ALCC are important drivers of this change, contributing 56% and 40%, respectively. The fact that these two contributions almost add up to 100% can be understood from the observation that agriculture was established predominantly in regions with high plant productivity, and in such regions dust emissions are per se low. Accordingly, natural and agricultural source regions are geographically distinct. In addition, this result indicates that climate change had no significant effect on dust emissions from agricultural lands. This could change in the future since today agricultural areas are much more expanded than in the late nineteenth century.

The main result of our study is the almost equal importance of climate change and anthropogenic land cover change for changes in dust emissions between the late 19th and the beginning of the 21st century. One can speculate that this will change in the future because agricultural expansion should stagnate according to recent land cover projections [*Hurtt et al.*, 2011]. If so, climate change should dominate changes of future dust emissions. This will be investigated in upcoming studies. But based on our results, we clearly recommend to account for both, anthropogenic land cover changes and climate changes when estimating changes in dust concentrations.

On a regional basis, the relative contribution of CC and ALCC vary. As in the past, North Africa is dominated today by natural emissions. Accordingly, our simulations show that here the 20th century increase in dust emissions and burden is caused by CC. In Australia, the increase in dust emissions and burden is mainly driven by ALCC. A mixed situation is found for Asia and North America, where both ALCC and CC contribute significantly to changes in dust emissions. In terms of radiative forcing, we obtain a global change of $-0.14\,W/m^2$ between the late nineteenth century and today.

We compared our regional changes in dust deposition and emissions with previous estimates based on the work of, e.g., *Mahowald et al.* [2010], *Neff et al.* [2008], and *Mulitza et al.* [2010]. For many regions of the world, *Mahowald et al.* [2010] reported rather small changes over the twentieth century but noted a large decadal variability, a feature we cannot investigate in our current setup. Our simulated changes in dust emissions do not always agree with the finding of *Mahowald et al.* [2010]. We note however that most of these previous estimates are based on paleorecords of dust deposition. Our model often simulates substantial spatial variations in dust deposition changes, even at continental scales (Figure 11), which questions the representativeness of changes in regional dust emission inferred from point measurements of dust deposition records. Further work is needed to reconcile these contrasting results.

Acknowledgments
The authors thank the Editor Steve Ghan and three anonymous reviewers for their useful comments, which helped us a lot to improve the paper. Further, we thank the AERONET Principal Investigators: J. Prospero and J. Savoie (University of Miami), the CALIOP, MODIS, and MISR teams for acquiring, processing, and providing data. In addition, we thank C. Siegenthaler-Le Drian (C2SM-ETH Zurich) for her technical support. The ECHAM-HAMMOZ model is developed by a consortium composed of ETH Zurich, Max Planck Institut für Meteorologie, Forschungszentrum Jülich, University of Oxford, and the Finnish Meteorological Institute and managed by the Center for Climate Systems Modeling (C2SM) at ETH Zurich. The simulations were performed at the Swiss National Computing Center (CSCS). The simulation output is available on request at tanja.stanelle@env.ethz.ch. This work is supported by the EU FP7 IP PEGASOS (FP7-ENV-2010/265148).

References

Baker, J. B., R. J. Southard, and J. P. Mitchell (2005), Agricultural dust production in standard and conservation tillage systems in the San Joaquin Valley, *J. Environ. Qual.*, *34*, 1260–1269, doi:10.2134/jeq2003.0348.

Bou Karam, D., C. Flamant, P. Tulet, J.-P. Chaboureau, A. Dabas, and M. C. Todd (2009), Estimate of Saharan dust emissions in the intertropical discontinuity region of the West African monsoon, *J. Geophys. Res.*, *114*, D13106, doi:10.1029/2008JD011444.

Boucher, O. (2013), Clouds and Aerosols, in *Climate Change 2013: The Physical Science Basis. Contribution of Working Group I to the Fifth Assessment Report of the Intergovernmental Panel on Climate Change*, edited by T. F. Stocker et al., Cambridge Univ. Press, Cambridge, U. K., and New York.

Braswell, B. H., D. S. Schimel, E. Linder, and B. Moore (1997), The response of global terrestrial ecosystems to interannual temperature variability, *Science*, *278*, 870–872, doi:10.1126/science.278.5339.870.

Bunn, J. A. (1997), Alternative beliefs about conservation practices and soil-productivity relationships, and the long-run outlook for agriculture on the southern Texas High Plains, *J. Agric. Appl. Econ.*, *30*, 339–351.

Cheng, T., Y. Peng, J. Feichter, and I. Tegen (2008), An improvement on the dust emission scheme in the global aerosol-climate model ECHAM5-HAM, *Atmos. Chem. Phys.*, *8*, 1105–1117, doi:10.5194/acp-8-1105-200.

Clausnitzer, H., and M. J. Singer (1996), Respirable-dust production from agricultural operations in the Sacramento Valley, *J. Environ. Qual.*, *25*, 877–884, doi:10.2134/jeq1996.00472425002500040032x.

Dentener, F. J., G. R. Carmichael, Y. Zhang, J. Lelieveld, and P. J. Crutzen (1996), Role of mineral aerosol as a reactive surface in the global troposphere, *J. Geophys. Res.*, *101*, 22,869–22,889, doi:10.1029/96JD01818.

de Noblet-Ducoudré, N., et al. (2012), Determining robust impacts of land-use-induced land cover changes on surface climate over North America and Eurasia: Results from the first set of LUCID experiments, *J. Clim.*, *25*, 3261–3281, doi:10.1175/JCLI-D-11-00338.1.

Diner, D. J., et al. (2001), MISR level 2 aerosol retrieval algorithm theoretical basis, JPL-D11400.

Drury, E., D. J. Jacob, J. Wang, R. J. D. Spurr, and K. Chance (2008), Improved algorithm for MODIS satellite retrievals of aerosol optical depths over western North America, *J. Geophys. Res.*, *113*, D16204, doi:10.1029/2007JD009573.

Engelstaedter, S., I. Tegen, and R. Washington (2006), North African dust emissions and transport, *Earth Sci. Rev.*, *79*(1–2), 73–100, doi:10.1016/j.earscirev.2006.06.004.

Fiorino, M. (2000), AMIP II sea surface temperature and sea ice concentration observations. [Available at http://www-pcmdi.llnl.gov/projects/amip/AMIP2EXPDSN/BCS_OBS/amip2_bcs.htm.]

Forster, P., et al. (2007), Changes in atmospheric constituent and in radiative forcing, in *Climate Change 2007: The Physical Basis, Contribution of Working Group I to the Fourth Assessment Report of the Intergovernmental Panel on Climate Change*, Cambridge Univ. Press, Cambridge, U. K., and New York.

Gillette, D. A. (1988), Threshold friction velocities for dust production for agricultural soils, *J. Geophys. Res.*, *93*(D10), 12,645–12,662, doi:10.1029/JD093iD10p12645.

Ginoux, P., M. Chin, I. Tegen, J. M. Prospero, B. Holben, O. Dubovik, and S.-J. Lin (2001), Sources and distributions of dust aerosols simulated with the GOCART model, *J. Geophys. Res.*, *106*(D17), 20,255–20,273, doi:10.1029/2000JD000053.

Ginoux, P., J. M. Prospero, T. E. Gill, N. C. Hsu, and M. Zhao (2012), Global-scale attribution of anthropogenic and natural dust sources and their emission rates based on MODIS Deep Blue aerosol products, *Rev. Geophys.*, *50*, RG3005, doi:10.1029/2012RG000388.

Granier, C., et al. (2011), Evolution of anthropogenic and biomass burning emissions of air pollutants at global and regional scales during the 1980–2010 period, *Clim. Change*, *109*(1–2), 163–190, doi:10.1007/s10584-011-0154-1.

Grantz, D. A., D. L. Vaughn, R. J. Farber, B. Kim, T. Van Curen, and R. Campbell (1998), Wind barriers offer short-term solution to fugitive dust, *Calif. Agric.*, *52*(4), 14–18, doi:10.3733/ca.v052n04p14.

Holben, B. N., et al. (1998), AERONET—A federated instrument network and data archive for aerosol characterization, *Remote Sens. Environ.*, *66*(1), 1–16.

Holben, B. N., et al. (2001), An emerging ground-based aerosol climatology: Aerosol optical depth from AERONET, *J. Geophys. Res.*, *106*(D11), 12,067–12,097, doi:10.1029/2001JD900014.

Hsu, N. C., S.-C. Tsay, M. King, and J. R. Herman (2004), Aerosol properties over bright-reflecting source regions, *IEEE Trans. Geosci. Remote Sens.*, *42*, 557–569, doi:10.1109/TGRS.2004.824067.

Huneeus, N., et al. (2011), Global dust model intercomparison in AeroCom phase I, *Atmos. Chem. Phys.*, *11*, 7781–7816, doi:10.5194/acp-11-7781-2011.

Hunt, W. H., D. M. Winker, M. A. Vaughan, K. A. Powell, P. L. Lucker, and C. Weimer (2009), CALIPSO lidar Description and performance assessment, *J. Atmos. Oceanic Technol.*, *26*(7), 1214–1228.

Hurtt, G. C., et al. (2011), Harmonization of land-use scenarios for the period 1500–2100: 600 years of global gridded annual land-use transitions, wood harvest, and resulting secondary lands, *Clim. Change*, *109*, 117–161, doi:10.1007/s10584-011-0153-2.

Jickells, T., Z. An, and K. Anderson (2005), Global iron connections between dust, ocean biogeochemistry and climate, *Science*, *308*, 67–71, doi:10.1126/science.1105959.

Jung, M., K. Henkel, M. Herold, and G. Churkina (2006), Exploiting synergies of global land cover products for carbon cycle modeling, *Remote Sens. Environ.*, *101*, 534–553, doi:10.1016/j.rse.2006.01.020.

King, M. D., Y. J. Kaufman, W. P. Menzel, and D. Tanrè (1992), Remote sensing of cloud, aerosol, and water vapor properties from the Moderate Resolution Imaging Spectrometer (MODIS), *IEEE Trans. Geosci. Remote Sens.*, *30*(1), 2–27.

King, M. D., W. P. Menzel, Y. J. Kaufman, D. Tanrè, B. C. Gao, S. Platnick, S. A. Ackerman, L. A. Remer, R. Pincus, and P. A. Hubanks (2003), Cloud and aerosol properties, precipitable water, and profiles of temperature and humidity from MODIS, *IEEE Trans. Geosci. Remote Sens.*, *41*, 442–458.

Kok, J. F. (2011), Does the size distribution of mineral dust aerosols depend on the wind speed at emission?, *Atmos. Chem. Phys.*, *11*, 10,149–10,156, doi:10.5194/acp-11-10149-2011.

Koven, C. D., and I. Fung (2008), Identifying global dust source areas using high-resolution land surface form, *J. Geophys. Res.*, *113*, D22204, doi:10.1029/2008JD010195.

Lamarque, J.-F., et al. (2010), Historical (1850–2000) gridded anthropogenic and biomass burning emissions of reactive gases and aerosols: Methodology and application, *Atmos. Chem. Phys. Discuss.*, *10*, 4963–5019, doi:10.5194/acpd-10-4963-2010.

Lee, J. A., K. A. Wigner, and J. M. Gregory (1993), Drought, wind and blowing dust on the southern High Plains of the United States, *Phys. Geogr.*, *14*, 56–67, doi:10.1080/02723646.1993.10642467.

Levy, R. C., L. A. Remer, R. G. Kleidman, S. Mattoo, C. Ichoku, R. Kahn, and T. F. Eck (2010), Global evaluation of the Collection 5 MODIS dark-target aerosol products over land, *Atmos. Chem. Phys.*, *10*, 10,399–10,420, doi:10.5194/acp-10-10399-2010.

Lohmann, U., P. Stier, C. Hoose, S. Ferrachat, S. Kloster, E. Roeckner, and J. Zhang (2007), Cloud microphysics and aerosol indirect effects in the global climate model ECHAM5-HAM, *Atmos. Chem. Phys.*, *7*, 3425–3446, doi:10.5194/acp-7-3425-2007.
Mahowald, N., et al. (2009), Atmospheric Iron deposition: Global distribution, variability and human perturbations, *Annu. Rev. Mar. Sci.*, *1*, 245–278, doi:10.1146/annurev/marine.010908.163727.
Mahowald, N. M., and C. Luo (2003), A less dusty future?, *Geophys. Res. Lett.*, *30*(17), 1903, doi:10.1029/2003GL017880.
Mahowald, N. M., G. D. R. Rivera, and C. Luo (2004), Comment on "Relative importance of climate and land use in determining present and future global soil dust emission", *Geophys. Res. Lett.*, *31*, L24105, doi:10.1029/2004GL021272.
Mahowald, N. M., et al. (2010), Observed 20th century desert dust variability: Impact on climate and biogeochemistry, *Atmos. Chem. Phys.*, *10*, 10,875–10,893, doi:10.5194/acp-10-10875-2010.
Marticorena, B., and G. Bergametti (1995), Modeling the atmospheric dust cycle: 1. Design of a soil-derived dust emission scheme, *J. Geophys. Res.*, *100*, 16,415–16,430, doi:10.1029/95JD00690.
Marticorena, B., G. Bergametti, B. Aumont, Y. Callot, C. N'Doumè, and M. Legrand (1997), Modeling the atmospheric dust cycle: 2. Simulations of Saharan dust sources, *J. Geophys. Res.*, *102*, 4387–4404, doi:10.1029/96JD02964.
Moullin, C., and L. Chiapello (2006), Impact of human-induced desertification on the intensification of the Sahel dust emission and export over the last decades, *Geophys. Res. Lett.*, *33*, L18808, doi:10.1029/2006GL025923.
Mulitza, S., et al. (2010), Increase in African dust flux at the onset of commercial agriculture in the Sahel region, *Nature*, *466*, 226–228, doi:10.1038/nature09213.
Neff, J. C., A. P. Ballantyne, H. L. Farmer, N. M. Mahowald, J. L. Conroy, C. C. Landry, J. T. Overpeck, T. H. Painter, C. R. Lawrence, and R. L. Reynolds (2008), Increasing eolian dust deposition in the western United States linked to human activity, *Nat. Geosci.*, *1*(3), 189–195, doi:10.1038/ngeo133.
Neff, J., R. Reynolds, J. Belnap, and P. Lamothe (2005), Multi-decadal impacts of grazing on soil physical and biogeochemical properties in southeast Utah, *Ecol. Appl.*, *15*, 87–95, doi:10.1890/04-0268.
Nordstrom, K. F., and S. Hotta (2004), Wind erosion from cropland in the USA: A review of problems, solutions and prospects, *Geoderma*, *121*, 157–167, doi:10.1016/jgeoderma.2003.11.012z.
Prospero, J. M., P. Ginoux, O. Torres, S. E. Nicholson, and T. E. Gill (2002), Environmental characterization of global sources of atmospheric soil dust identified with the NIMBUS 7 Total Ozone Mapping Spectrometer (TOMS) absorbing aerosol product, *Rev. Geophys.*, *40*(1), 1002, doi:10.1029/2000RG000095.
Prospero, J. M., W. M. Landing, and M. Schulz (2010), African dust deposition to Florida: Temporal and spatial variability and comparison to models, *J. Geophys. Res.*, *115*, D13304, doi:10.1029/2009JD012773.
Ramankutty, N., and J. A. Foley (1999), Estimating historical changes in global land cover: Croplands from 1700 to 1992, *Global Biogeochem. Cycles*, *13*(4), 997–1027, doi:10.1029/1999GB900046.
Reick, C. H., T. Raddatz, V. Brovkin, and V. Gayler (2013), Representation of natural and anthropogenic land cover change in MPI-ESM, *J. Adv. Model. Earth Syst.*, *5*, 459–482, doi:10.1002/jame.20022.
Ridley, D. A., C. L. Heald, J. R. Pierce, and M. J. Evans (2013), Toward resolution-independent dust emissions in global models: Impacts on the seasonal and spatial distribution of dust, *Geophys. Res. Lett.*, *40*, 2873–2877, doi:10.1002/grl.50409.
Ryder, C. L., E. J. Highwood, T. M. Lai, H. Sodeman, and J. H. Masham (2013), Impact of atmospheric transport on the evolution of microphysical and optical properties of Saharan dust, *Geophys. Res. Lett.*, *40*, 2433–2438, doi:10.1002/grl.50482.
Shannon, S., and D. J. Lunt (2011), A new dust cycle model with dynamic vegetation: LPJ-dust version 1.0, *Geosci. Model Dev.*, *4*, 85–105, doi:10.5194/gmd-4-85-2011.
Stevens, B., et al. (2013), Atmospheric component of the MPI-M Earth System Model: ECHAM6, *J. Adv. Model. Earth Syst.*, *5*(2), 146–172, doi:10.1002/jame.20015.
Stier, P., et al. (2005), The aerosol-climate model ECHAM5-HAM, *Atmos. Chem. Phys.*, *5*, 1125–1156, doi:10.5194/acp-5-1125-200.
Strong, C. L., K. Parsons, G. H. McTainsh, and A. Sheehan (2011), Dust transporting wind systems in the lower Lake Eyre Basin, Australia: A preliminary study, *Aeolian Res.*, *2*, 205–214, doi:10.1016/j.aeolia.2010.11.001.
Tegen, I., and I. Fung (1995), Contribution to the atmospheric mineral aerosol load from surface modification, *J. Geophys. Res.*, *100*, 18,707–18,726, doi:10.1029/95JD02051.
Tegen, I., S. P. Harrison, K. Kohfeld, and I. C. Prentice (2002), Impact of vegetation and preferential source areas on global dust aerosol: Results from a model study, *J. Geophys. Res.*, *107*(D21), 4576, doi:10.1029/2001JD000963.
Tegen, I., M. Werner, S. P. Harrison, and K. E. Kohfeld (2004), Relative importance of climate and land use in determining present and future global soil dust emission, *Geophys. Res. Lett.*, *31*, L05105, doi:10.1029/2003GL019216.
Tibke, G. (1988), Basic principles of wind erosion control, *Agric. Ecosyst. Environ.*, *22/23*, 103–122, doi:10.1016/0167-8809(88)90011-4.
Timmreck, C., and M. Schulz (2004), Significant dust simulation differences in nudged and climatological operation mode of the AGCM ECHAM, *J. Geophys. Res.*, *109*, D13202, doi:10.1029/2003JD004381.
Uri, N. D. (1999), Factors affecting the use of conservation tillage in the United States, *Water Air Soil Pollut.*, *116*, 621–638.
Van Vuuren, D. P., et al. (2011), The representative concentration pathways: An overview, *Clim. Change*, *109*, 5–31, doi:10.1007/s10584-011-0148-z.
Vignati, E., J. Wilson, and P. Stier (2004), M7: An efficient size-resolved aerosol microphysics module for large-scale aerosol transport models, *J. Geophys. Res.*, *109*, D22202, doi:10.1029/2003JD004485.
Zender, C. S., H. S. Bian, and D. Newman (2003), Mineral Dust Entrainment and Deposition (DEAD) model: Description and 1990s dust climatology, *J. Geophys. Res.*, *108*(D14), 4416, doi:10.1029/2002JD002775.
Zender, C. S., R. L. Miller, and I. Tegen (2004), Quantifying mineral dust mass budgets: Terminology, constraints, and current estimates, *Eos Trans. AGU*, *85*, 509–512, doi:10.1029/2004EO480002.
Zhang, K., et al. (2012), The global aerosol-climate model ECHAM-HAM, version 2: Sensitivity to improvements in process representations, *Atmos. Chem. Phys. Discuss.*, *12*, 7545–7615, doi:10.5194/acpd-12-7545-2012.